Master's Thesis

Dynamic monitoring of neuronal activities in brain slice and probe-based optical stimulation of primary cultured neuron

Geonho Choi

Department of Biomedical Engineering

Graduate School of UNIST

2018

Dynamic monitoring of neuronal activities in brain slice and probe-based optical stimulation of primary cultured neuron

Geonho Choi

Department of Biomedical Engineering

Graduate School of UNIST

Dynamic monitoring of neuronal activities in brain slice and probe-based optical stimulation of primary cultured neuron

A thesis/dissertation
submitted to the Graduate School of UNIST
in partial fulfillment of the
requirements for the degree of
Master of Science

Geonho Choi

11. 23. 2017

Approved by

Advisor
Woonggyu Jung

Dynamic monitoring of neuronal activities in brain slice and probe-based optical stimulation of primary cultured neuron

Geonho Choi

This certifies that the thesis/dissertation of Geonho Choi is approved.

11/23/2017

signature

Advisor: Woonggyu Jung

signature

Thesis Committee: Cheol-Min Ghim

signature

Thesis Committee: Chan-Young Park

ABSTRACT

In this study, we introduce the novel image-guided recording system (IGRS) to interpret the dynamics and distribution of neuronal activities in temporal and spatial scale. Our device was designed to integrate the microelectrode array (MEA) and optical coherence tomography (OCT) at the single-body upright microscope, which enables to image the volumetric brain anatomy and measure multi-sites neuronal activities simultaneously. Using IGRS, we established the time-series mapping protocol on the 3D brain structure after intensive image and signal processing. In order to evaluate the performance of IGRS, neuronal activities of hippocampal region in the brain slice were monitored, and corresponding spatial and temporal mapping was intuitively visualized. Through continuative experiment, it was found that our tool could successfully provide the comprehensive information regarding to excitable neuronal signals.

In the aspect of stimulation research, various optical methods have been introduced recently as an alternative technique because of spatial resolution, multiple stimulation as well as non-invasive manner. Among optical stimulation methods, single-photon stimulation based on caged glutamate is one of well-known technique which uses photolysis to release neurotransmitter like a glutamate. Through the preliminary research, we could predict the condition of action potential firing using a photolysis simulation. Based on it, we introduce ball-lensed probe which have several advantages to stimulate neurons. This device is not expensive and can be easily used than commercial light source because it is made of laser module. And it is useful to apply for tissue sample and multi-stimulation because of probe type.

In summary, IGRS and ball-lensed probe would be very efficient tool to investigate and stimulate neuronal activities and connectivity in various fields.

Keywords: Microelectrode arrays, Optical Coherence Tomography, Single-photon stimulation, Caged glutamate.

CONTENTS

LIST OF FIGURES

Ⅰ. Introduction

1.1. Motivation

Many researchers have tried to find the reason, symptom and treatment method of neuronal disease like Epilepsy, Alzheimer's disease and so on. In order to figure out, they have used disease model of rat and mouse in hippocampus region **[1-4]**. The reasons why the hippocampus is important in this field are that the hippocampus plays key roles in learning and memory **[5-7]**.

However, monitoring platform is not enough to observe the neuronal activities and physiological information in hippocampus region since it provides them respectively. In order to overcome the limitation, we developed Image-guided Recording System (IGRS) based on the combination of MEA and OCT. For practical interpretation of neuronal activities on brain structure image, we demonstrate experiment protocol which includes OCT imaging, image processing, neuronal activities recording, signal processing and mapping. We finally evaluate its performance while applying it to register spatial and temporal mapping of neuronal activities in hippocampal region of the brain slice.

After the monitoring system was prepared, we have focused on single-photon stimulation method which uses photolysis to release neurotransmitter. In preliminary research, we proposed the photolysis equation consists of the concentration of glutamate and optical stimulation parameters which include wavelength, intensity, and exposure time to adjust experimental conditions and predict corresponding neuronal activity **[8]**. However, this system is expensive and low accessibility to other devices. Therefore, we developed probe-based optical stimulator which has various advantages like accessibility, cost efficiency, and portability.

Ⅱ. Image-guided recording system for spatial and temporal mapping of neuronal activities in brain slice

2.1. Introduction

In neuroscience, investigating the neuronal connectivity and dynamics in the brain is essential component to understand its specific function. To date, electrophysiological technology has made big contribution to study functional connectivity, while recording intracellular and extracellular activities from excitable neurons **[9-11]**. Microelectrode arrays (MEAs) is an emerging electrophysiological device which allows multi-readout extracellular communications, non-invasively. The simultaneous recording and stimulation of large populations of neurons with long-term reliability is the most unique feature of MEA **[12]**. Since MEA also doesn't requires sophisticated skills and environments compared to patch electrodes, it has been used in wide-range of applications **[13-14]**. At presents, many research groups have still made effort to develop advanced MEAs including the cost-effective device and high density of electrodes for presenting the detailed neuronal connectivity with the sufficient temporal resolution **[13, 15-16]**. Even though valuable information can be obtained by improved MEA device, there is still technical challenge for dealing with signal processing of massive data acquired from dense electrodes. In particular, it is significantly required to devise the efficient registration of neuronal signals in temporal and spatial scale while avoiding conventional method, manual drawing and mapping **[17-19]**.

Here, we demonstrate image-guided MEA recording system (IGRS) in order to provide the comprehensive and intuitive neuronal mapping in brain slice. Our system is based on the optical coherence tomography (OCT) integrated to typical MEA platform. OCT is non-invasive imaging modality which allows real-time cross-sectional tissue structure with micrometer-scale high resolution in real-time **[20-21]**. Since OCT relies on the inherent differences in optical scattering within tissue, cross-sectional or enface images can be generated without the addition of exogenous stains or probes. After invention of OCT, it has been intensively utilized in medical fields for diagnosing a variety of tissue abnormalities in early stage. In last few years, the use of OCT for visualizing anatomical structure of brain tissue was getting increased **[22-24]**. Previous works including recent our work clearly presented that OCT has enough resolution and contrast to delineate the multi-scale neuronal morphologies of brain slice. **[22]** On the other hands, few studies have reported the usefulness of OCT for confirming the presence and attachment of implanted single micro-electrode or MEA in brain and retina. Thus, OCT has clear feasibility and potential to visualize between MEA and brain structure. However, further expansion to link neuronal activity has not been carried out despite the clear need **[25]**.

In this work, we first introduce image-guided recording system (IGRS) based on the combination of MEA and OCT. For practical interpretation of neuronal activities on brain structure image, we

demonstrate experiment protocol which includes OCT imaging, image processing, neuronal activities recording, signal processing and mapping. We finally evaluate its performance while applying it to register spatial and temporal mapping of neuronal activities in hippocampal region of the brain slice.

2.2. Methods and Materials

2.2.1 Swept Source Optical Coherence Tomography

Home-built imaging system is combined with upright microscope and SS-OCT (Swept Source Optical Coherence Tomography) to acquire 3D brain structure information. A schematic diagram of the experiment set-up is shown in **Figure 1-1**. The SS-OCT system has a center wavelength of 1060nm, bandwidth of 100nm and sweep rate of 100kHz. The axial and transverse resolutions of a 2D image are ~5 μm and ~6 μm, respectively. The beam emitted from swept source was split by 50:50 fiber-optics coupler, guiding one to the reference mirror and the other toward to the dual-axis galvano mirrors to scan the brain slice. After that, laser was led to the tilted mirror which was placed between an ocular and objective lens (4×; NA=0.1) in the body of upright microscope. After the reflected laser from sample and reference converged at coupler together, it generated interference which has depth resolved frequency signal. Through the photo detector, the optical interference signal is converted into analog electrical signal and recorded through digitizer. Therefore, this setup enables users to observe the sample as well as take an OCT image simultaneously.

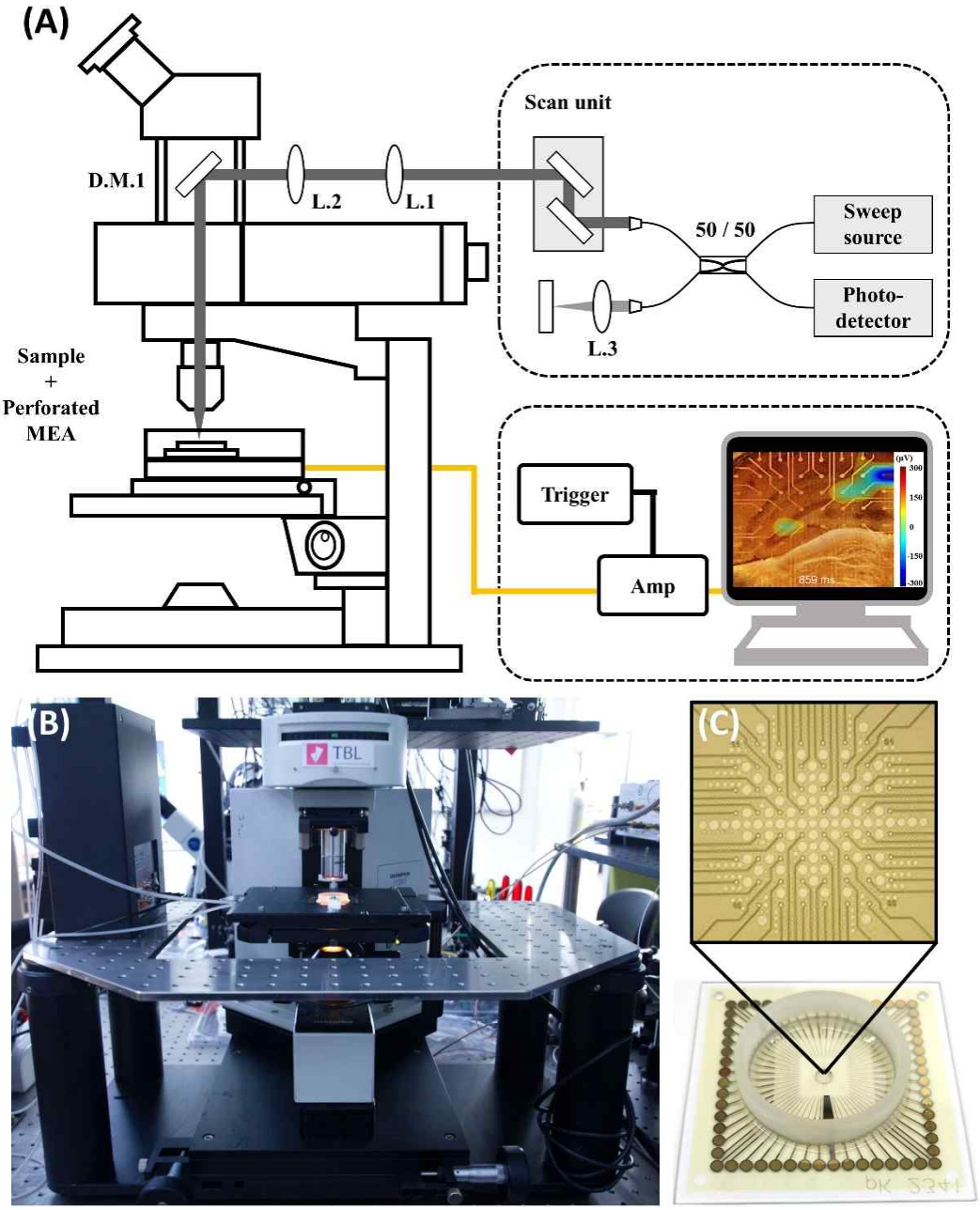

Figure 1-1. Experimental set-up.

(A) Schematic diagram of Image-guided recording system (IGRS). (B) IGRS consists of SS-OCT imaging system and pMEA electrophysiological recording system. Optical path was inserted into the body of upright microscopy to acquire 3D image (D.M: Dichroic mirror; L1, L2, L3: Lens). Acquired signals from pMEA was amplified and analyzed in control module (Amp: Amplifier). (C) pMEA has lots of perforated holes and 60 electrodes lines covered in 2 mm × 2 mm.

2.2.2 Extracellular Recording

For neuronal recording, we utilized a 60-channel extracellular recording system (USB-ME64, Multichannel systems, Germany) mounted on the stage of upright microscope. All local field potentials (LFPs) and action potentials (AP) were measured at a 10kHz sampling rate using the MC_Rack (Multichannel Systems, Germany) software. In this program, we set 60 Hz high-pass filter as a default due to excluding AC frequency from voltage source. For AP analysis, 300 Hz high-pass filter was added to detect it and these signals were extracted by negative amplitude threshold.

The experiment set-up was built around an inverted microscope (IX70 Olympus, Japan) including a customized culture chamber (Live cell instruments, Korea), 37ºC temperature controller and a humidified 5% CO_2 gas inlet in order to enhance viability and stabilization of brain slice.

In the part of electrophysiological recording device, pMEA (perforated Micro-Electrode Array) was placed on the stage of microscope to get the extracellular signals of neurons in the brain slice. It was composed of an 8 × 8 array with reference electrode in Ch.15. And diameter of each electrode was 30 μm and each distance of individual electrodes was 200 μm. In addition, pMEA has a lot of holes which enable a sample to be clearly attached to the surface of electrodes when the negative pressure was applied by syringe pump. If the sample was not fully contacted on the electrodes, the space between the sample and electrodes could be filled with solution. Then, it could raise the noise level and analysis of neuronal signals could be difficult because meaningful data were covered by noise.

2.2.3 Acute Brain Slice Preparation

Acute hippocampal brain slice was obtained from wild-type C57BL6 mice (4 ~ 8 weeks old). The animals are anesthetized with 2-Bromo-1,1,1-trifluoroethane (Sigma-Aldrich, UK) and decapitated. The brain was removed from skull and placed in oxygenated (95% O_2 / 5% CO_2) ice-cold (0 ~ 5°C) artificial cerebrospinal fluid (ACSF; 125 mM NaCl, 26 mM $NaHCO_3$, 25 mM glucose, 3.5 mM KCl, 2.4 mM $CaCl_2$, 1.3 mM $MgCl_2$, 1.2mN NaH_2PO_4; pH 7.2) during slicing step. The brain was cut with vibrating microtome (VT1000 S; Leica, Nussloch, Germany). Coronal slices (~400μm thickness) were incubated in oxygenated ACSF at temperature (32~35°C) for 30 min prior to using for experiments. After stabilizing sample, coronal brain slice was put on the surface of pMEA with oxygenated ACSF. And negative pressure was applied through a lot of holes by syringe pump **[26]**. Entire experiment and animal handling was carried out according to IACUC regulation in UNIST (UNISTIACUC-17-08).

To confirm the feasibility of extracellular recording of pMEA, 1mM 4-Aminopyridine (Sigma Aldrich) and 1 μM Tetrodotoxin (Sigma Aldrich) were used. 4-AP (4-Aminopyridine) is a voltage-gated K+ channel blocker that induces intense electrical discharges and seizure activity. And TTX (tetrodotoxin) is a voltage-gated Na+ channel blocker promptly eliminates neuronal firing of action potentials **[27-29]**.

2.3. Results

2.3.1 Images of Hippocampus with Thickness

In **Figure 1-2**, the images of brain slice in hippocampus region were acquired by upright microscope, inverted microscope and OCT. In 300 μm thickness, all imaging modality could provide the location of electrodes as well as information of tissue structure. As the thickness of hippocampus increase, the position of electrodes was not shown in upright microscope image and tri-synaptic structure was not shown in inverted microscope image, respectively. In case of OCT, both of information could be acquired regardless of sample thickness.

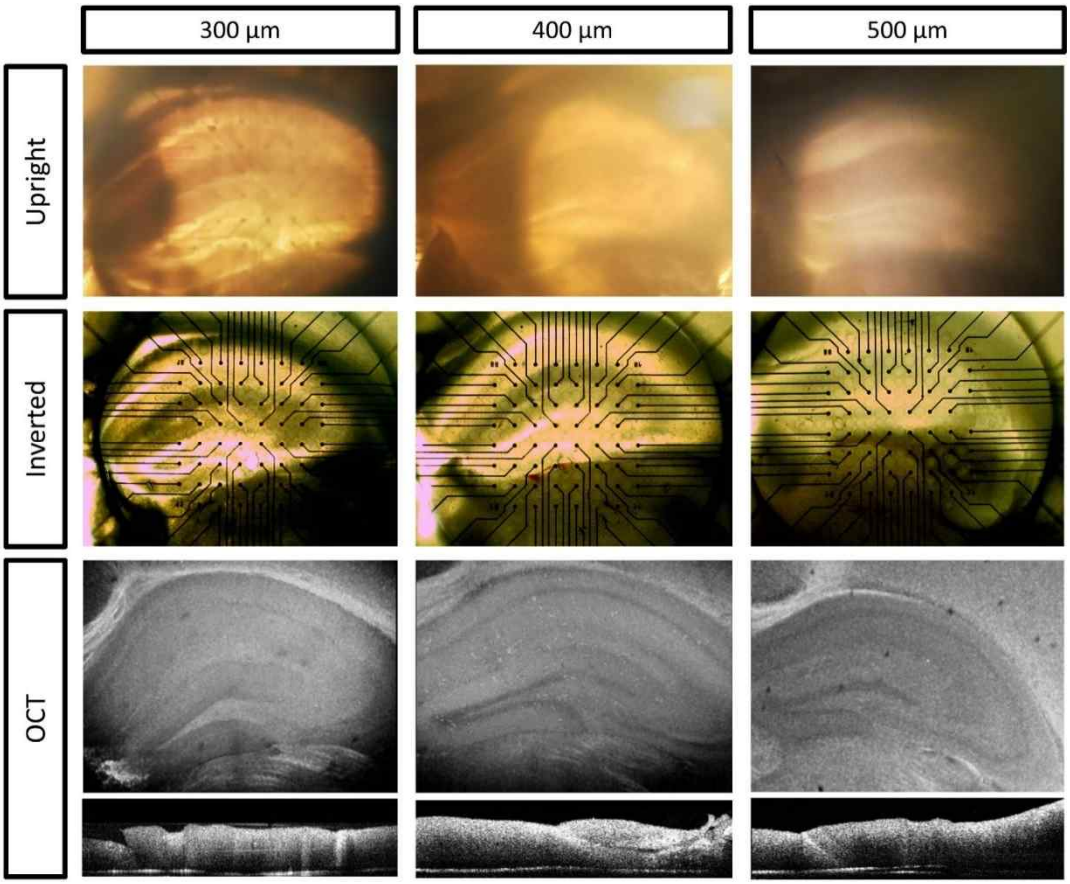

Figure 1-2. The comparison of brain slice images in hippocampus region using upright microscope, inverted microscope and OCT

2.3.2 Action Potentials

We did pharmacological experiment to demonstrate whether the signals which we acquired are real action potentials as comparison of number of spikes per min. As we mentioned above, 4-AP is a K+ channel blocker and causes epileptiform activity. In contrasts, TTX is Na+ channel blocker and inhibits firing of neuronal signals **[27]**.

In this experiment, brain slices were incubated in cold ACSF (0 ~ 5°C) to prevent excitotoxicity. Also, oxygen gas was supplied to the solution indirectly because the flow of it could make the sample damage and excitotoxic **[30]**. Then, one of them was placed on the pMEA with warm ACSF (32~35°C) and negative pressure was applied by syringe pump. At that time, if the force was too strong, the brain slice must be sucked through a lot of holes. Therefore, researchers had to observe the sample through eyepiece lens of microscopy and should raise it carefully. After 5 minutes for stabilization, the signals were recorded during 5 minutes with 300 Hz high-pass filter to detect action potentials in hippocampal region. And these spikes were sorted when its value exceeds -5 standard deviation.

As shown in **Figure 1-3**, the data were extracted as much as 1000 ms from original one in channel 58 and noise level was about ±10 μV. In case of normal condition, several spontaneous action potentials were observed in a second. However, the results of 4-AP and TTX showed remarkable difference of the number of spikes. As 4-AP was treated, a lot of bursts of the neuronal activities were detected. Contrarily, after TTX was added in this solution, only few spikes were checked in TTX condition.

Then, all APs were sorted and overlapped to check the shape of spikes in **Figure 1-3 (B)**. Totally, 2197 spikes were accumulated at channel 58 and black line was averaged signal during 5 min. In **Figure 1-3 (C)**, this graph indicated that average number of action potentials had obvious difference. When they were calculated, the channels which did not occur any peaks were removed to minimize quantitative error. If total spikes number was divided by the number of whole channels, the result must be distorted because the number of channels which did not have any signals were included. Therefore, averaged value was total number of spikes at activated electrodes divided by total number of activated electrodes.

Through these pharmacological experiments, we could find the change of neuronal activities which was related to the chemical condition. Using 4-AP, signals were activated and inhibited when TTX was added in same sample. It meant that we could believe the signals which we took and analyzed were neuronal activities.

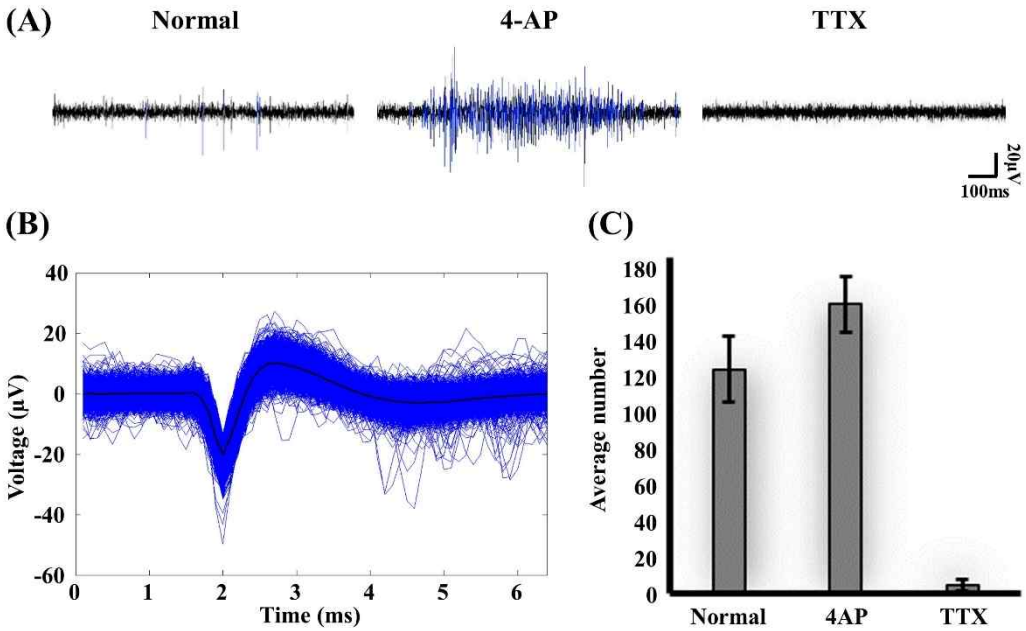

Figure 1-3. The results of action potentials in pharmacological experiment.

(A) Comparison of compressed graph of action potentials with normal, 4-AP and TTX treatment. All of spikes which exceed -5 standard deviation thresholds were expressed by blue color during 1000ms. (B) Sorted spikes from ch.58 was accumulated and black line was averaged data. (C) The average number of evoked spikes per min was plotted on graph for quantitative analysis (n=5).

2.3.3 OCT images of brain slice on MEA

The common way to observe the structure of brain slice is to use the upright microscope which can clearly visualize the surface of brain tissue as shown in **Figure 1-4 (A)**. However, it is limited uniformly to examine multi-sites electrodes below the specimen due to the different regional scattering properties of brain tissue. In particular, it is critical when the thickness of brain slice is typically above 400 μm. 3D OCT, visualizing the surface view as well as cross-sectional view, can be an alternative tool to overcome this limitation. Since OCT uses an infrared light, it inherently allows deep tissue imaging compared to a conventional light microscope. The typical penetration depth of OCT image is around 2-3 mm, which is enough to image electrodes beneath brain slice. In feasibility study, 50 mm focal length lens was used for the comparison with the bright-field microscope image while showing the entire brain slice on MEA in **Figure 1-4 (B)**. In addition, volumetric OCT image distinctly showed of hippocampus region covered in 2 mm × 2 mm with 4× objective lens while offering electrode distribution, as presented in **Figure 1-4 (C, D)**. In particular, the electrodes in OCT image was presented as strong white lines indicating high scattering property due to metal-coated layer of electrode. Since 3D OCT was able to visualize the formation of electrodes and brain tissue anatomy simultaneously, it helped well to adjust the loading position of sliced brain tissue on MEA where we would like to observe. It could also aid to construct electrodes-overlaid 3D brain tissue anatomy and neuronal signal map afterwards.

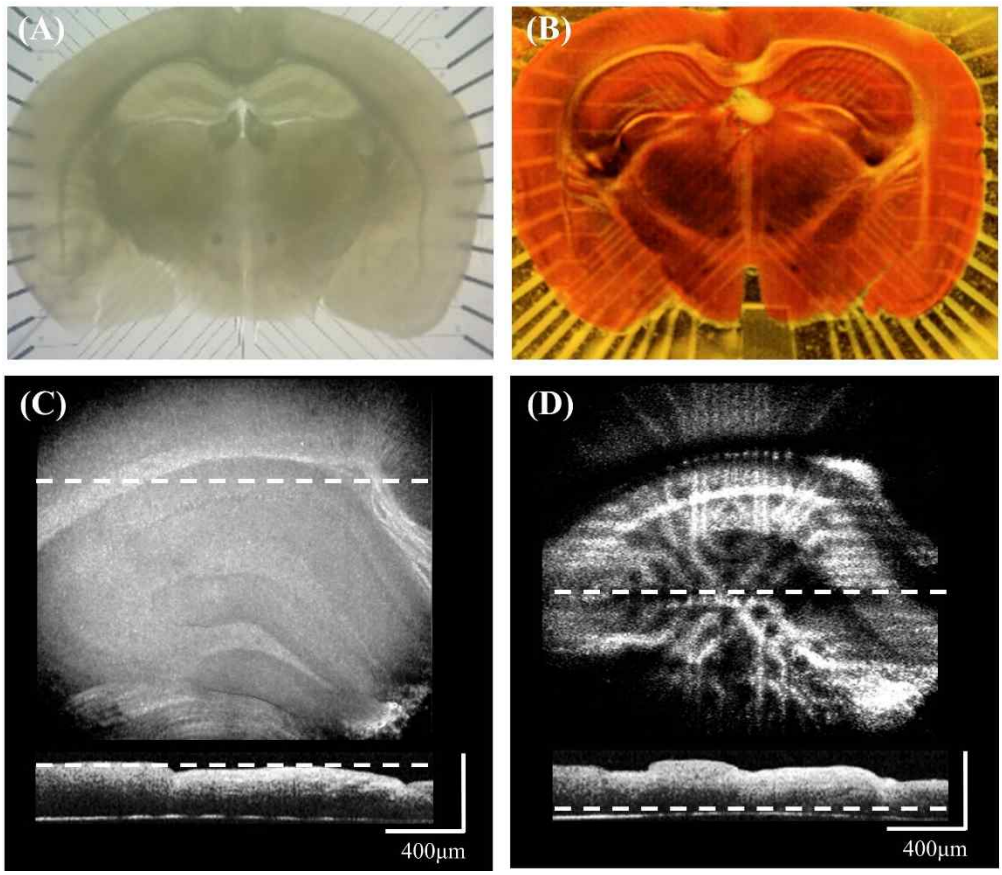

Figure 1-4. The brain slice images of bright-field microscope and OCT.

(A) Surface images of brain slice acquired from bright-field microscope, (B) 3D OCT image of brain slice. It visualizes the volumetric tissue as well as electrodes beneath the brain slice. (C, D) Brain tissue structure of hippocampus region in arbitrary direction and location with 4× objective lens. Dashed line indicates corresponding sectional images at yz and xy plane.

2.3.4 Spatial and temporal mapping protocol of IGRS

We developed the interpretation software of IGRS for spatial and temporal mapping of neuronal signals on OCT images using MATLAB as shown in **Figure 1-5**. The mapping protocol consists of 8 different steps including OCT imaging, image processing and signal processing. Since OCT image of electrodes with brain tissue in **Figure 1-4 (C, D)** looks blurry, we initially acquired pMEA image using OCT to provide clear electrodes image before loading brain tissue. Top-view OCT image regarding to pMEA well visualized both the perforated holes and multiple electrodes with 2 mm by 2 mm as presented in **Figure 1-5 (A)**. In order to extract the only electrodes, image segmentation processing including thresh-holding, transformation of a gray-scale, and binary conversion was executed. Resultant image of electrodes was visualized as presented in **Figure 1-5 (B)**.

After loading brain tissue on the pMEA, another OCT imaging was taken which visualized volumetric brain morphology as well as electrodes simultaneously (**Figure 1-5 (C)**). Since our OCT image identify the location of electrodes, we could confirm and match the exact position of brain tissue on the electrodes. Entire volumetric OCT images were projected from top-view in order to denote the brain anatomy and electrodes. **Figure 1-5 (D)** shows the projected OCT image visualizing hippocampal region of brain tissue as well as electrodes covering the scale of 2 mm × 2 mm × 400 μm. After projected OCT is ready, neuronal signals of brain slice were recorded by pMEA with 60 channels (**Figure 1-5 (E)**). Time-series neuronal signals acquired from each electrode were then converted as two-dimensional signal map. In order to produce color-coded signal map, neuronal signals were processed by bilinear interpolation which was required to make it more natural because the electrodes of MEA took the surrounding extracellular signals. In bilinear interpolation, it enables an area of unknown pixels between 2 × 2 electrodes to find the appropriate values of neuronal activities. Therefore, the area was represented by red or blue color depending on positive or negative values and each region of the point was easily distinguished in a color-coded signal map. Regional color-coded expressing the neuronal values were finally overlaid on the previous projection OCT image (**Figure 1-5 (F)**). In order to clearly visualize the anatomy of brain tissue morphology, color-coded neuronal signal map was adjusted by thresh-holding and transparency values (**Figure 1-5 (G)**). Time sequential two-dimensional IGRS map was finally reconstructed with repeated process (**Figure 1-5 (H)**).

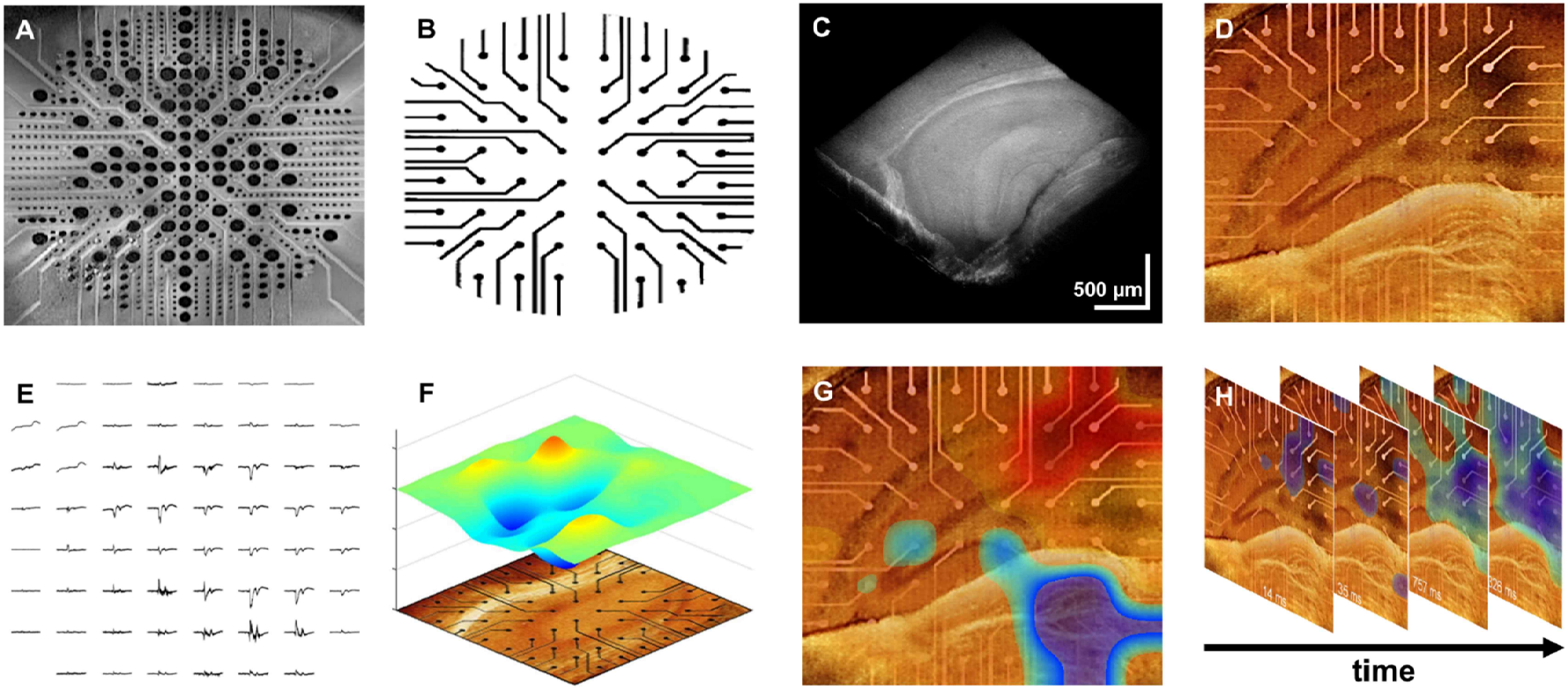

Figure 1-5. Spatial and temporal mapping protocol of IGRS.

(A) pMEA image acquired by OCT system before loading the brain tissue (dark dots: perforated holes, bright lines: electrodes). (B) Electrode image extracted by image segmentation processing. (C) 3D OCT image visualizing the volumetric hippocampus with electrodes (D) OCT projection image presenting the hippocampus morphology and extracted electrode (E) Neuronal activities recorded by pMEA in 60 channels. (F) Two-dimensional neuronal color map and its alignment with OCT image. (G) Overlaid color-coded map adjusted by thresh-holding and transparency values. (H) Time sequential IGRS maps.

2.3.5 *Measurement of neuronal activity using IGRS.*

As mentioned above, it was difficult to analyze the signals which were evoked simultaneously in a lot of channels using commercial program. Also, it became harder as the recording time increased because of the amount of data. Thus, it was poor to find where the electrical signals were originated from, how many them passed away through specific position and finally which point was destination. However, these limitations could be improved when we built mapping video using IGRS. IGRS which could show spatial and temporal information in sight was built by putting a series of spatial mapping image in order of the time. As shown **Figure 1-6~8**, we could build different type of mapping images depending on which data we used like action potentials and local field potentials in our system.

In **Figure 1-6**, action potential signals were acquired from MEA in 60 channels and mapping images based on these data in normal, 4-AP and TTX treatment. In order to verify the amount of APs, different channel blockers such as 1mM 4-Aminopyridine (4-AP) and 1 μM Tetrodotoxin (TTX) were used. 4-AP is a voltage-gated K+ channel blocker that induces intense electrical discharges and seizure activity. In other hands, TTX is a voltage-gated Na+ channel blocker promptly eliminates neuronal firing of action potentials. Each of the cases was recorded during 5 min and these were extracted as 1000 ms long. Comparing the results of **Figure 1-6 (A)**, mapping images could provide the information more easily because it was visual manner. We could find that the spontaneous activities evoked at right top side. And more signals induced by 4-AP were detected at more broad area. Moreover, the neuronal activities which were not evoked in normal case were activated on the left side of hippocampus area. After that, most of the signals were suppressed and disappeared due to TTX treatment. Therefore, it was very useful to observe the responses of nerve cells in brain slice about drug and toxin. Because it could offer the color-coded map for showing which position was affected and how many responses were generated with real tissue structure.

Local field potential (LFP) signals and waveforms acquired from DG, CA3 and CA1 region of hippocampus by MEA in 60 channels as shown in **Figure 1-7**. In the region of hippocampus, there was a tri-synaptic circuit which had been studied for many years. It had a primary route the signals passed from DG (Dentate Gyrus) to CA-3 (Cornu Ammonis-3) and CA-1 (Cornu Ammonis-1). Especially, within the Ammon's horn, there is a tri-synaptic glutamatergic circuit that connects dentate gyrus to CA3 (via mossy fibers), CA3 to CA1 (via Schaffer' collaterals) [31-33]. We could take the pattern of LFP propagation and evoked time using MEA. However, it was not enough to match the exact position as well as to figure out accurate propagation direction because MEA provided massive data of lots of electrode channels. Therefore, it meant that additional steps must be progressed to find the results we needed. In order to overcome these limitations and problems, we developed IGRS which can show the spatial and temporal map.

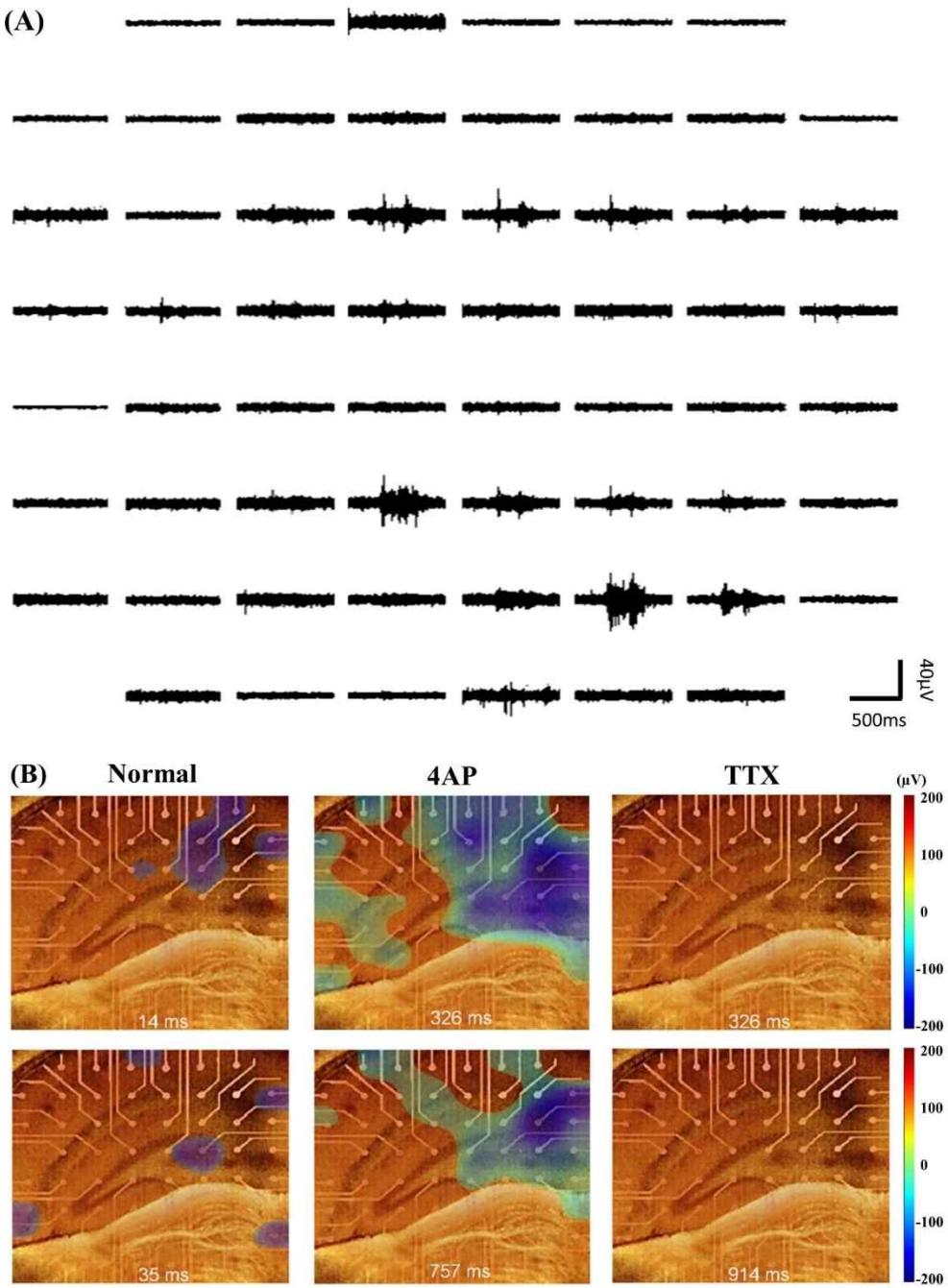

Figure 1-6. (A) Action potential signals acquired from MEA in 60 channels and (B) mapping image of action potentials with normal, 4-AP and TTX treatment.

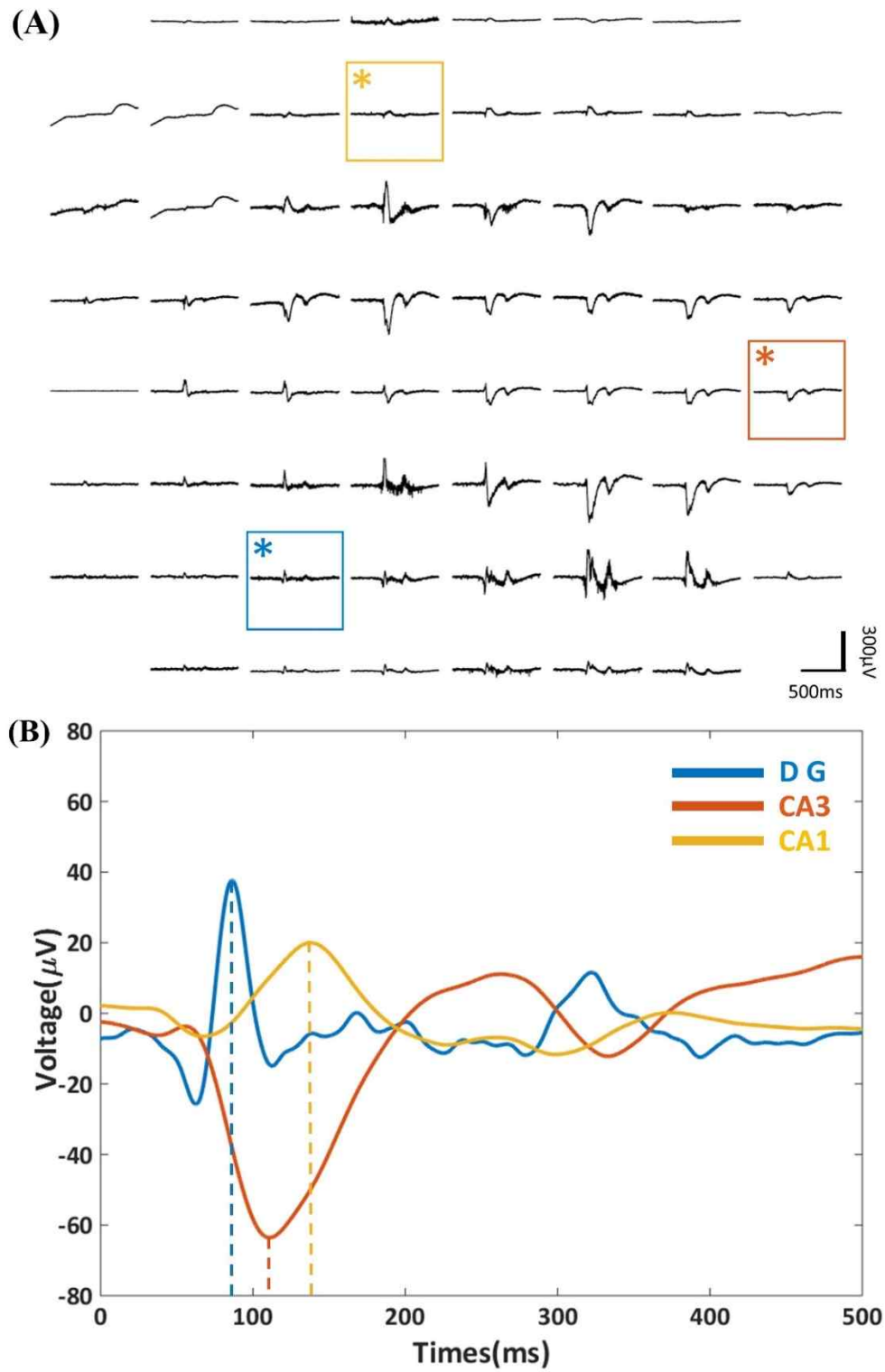

Figure 1-7. (A) Local field potential (LFP) signals acquired from MEA in 60 channels and (B) LFP signal waveforms acquired from DG, CA3 and CA1 region of hippocampus.

Figure 1-8 (B1-6) presents a time series of mapping images indicating the propagation of spontaneous LFPs along the tri-synaptic circuit. In the primary route, LFPs sequentially propagated from DG to CA3 and CA1. Using IGRS we observed well-known spatial and temporal activity in the tri-synaptic circuit for 5 minutes. Spontaneous LFPs were initially detected in the DG after 24 ms with about +221 μV. The value of LFPs in DG increased and had a maximum up to +293 μV, which was clearly reflected by the red color map of IGRS at 32 ms. At the same time, positive and negative signals begun to generate in CA3 as shown in **Figure 1-8 (B3)**. After 41 ms, the fully activated neuronal activities were displayed in all DG, CA3 and CA1 (**Figure 1-8 (B4)**). The LFPs of DG completely disappeared at 51 ms, whereas LFPs in CA3 and CA1 still remained and then decreased afterwards (**Figure 1-8 (B5-6)**). Through this experiment, we found that IGRS is a very promising tool to monitor dynamic signal flow over neuronal circuit due to the capability of accurate brain anatomy mapping with neuronal signals.

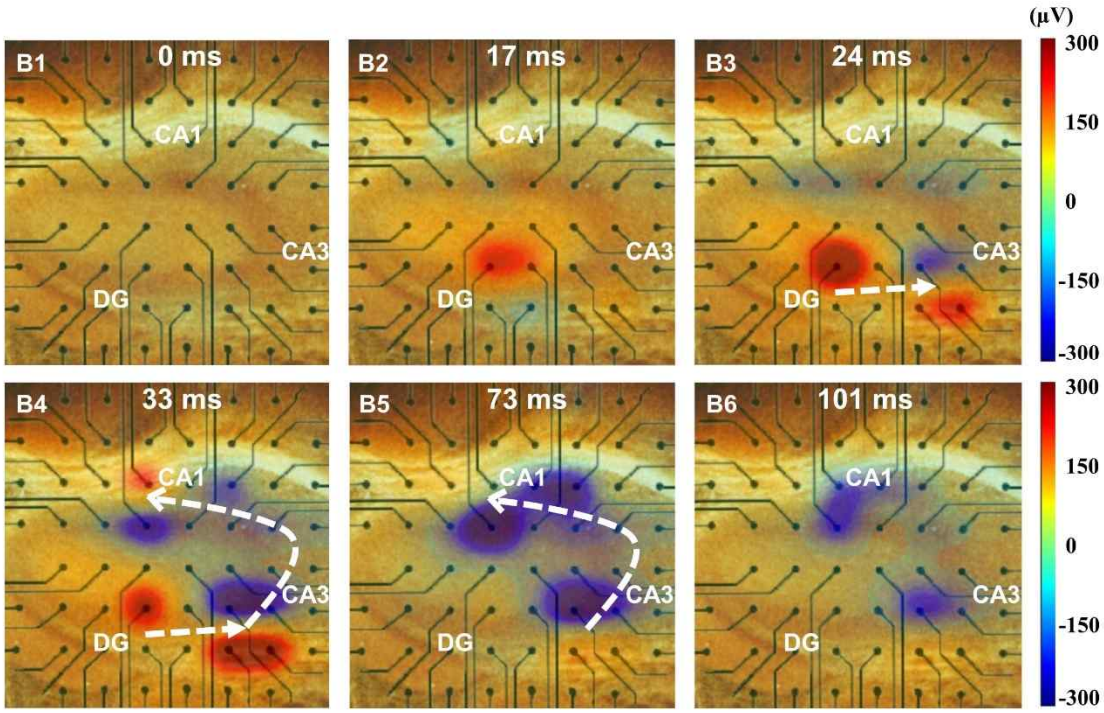

Figure 1-8. A series of LFPs mapping images showing the propagation of LFP through tri-synaptic circuit using IGRS.

2.3.6 Application for Electrical Stimulation

IGRS made it easy to identify defects of brain slice since our system was based on 3D OCT image. Using IGRS, we could find sample defects like holes in red rectangle boxes as shown in **Figure 1-9 (A, B)**. These defects were caused by syringe pump which applied negative pressure through lots of holes. If applied negative pressure was too high, brain slice was sucked through the perforated holes. Therefore, we could find sucked points at enface image and try to record neuronal signals after this sample check step to get better results. The condition of sample can be confirmed through our system.

In addition, IGRS could be applied for electrical stimulation research since it could provide 3D sample image as well as the neuronal activities using a spatial and temporal color-coded map. When we used external electrode to stimulate specific point, it was important to confirm where the spot was and how much the depth was. In **Figure 1-9 (C)** showed 3D hippocampus image with red colored external electrode. Also, the difference of depth was more remarkable but also accurate depth values based on pixel calculating as shown in **Figure 1-9 (D)**. Therefore, calculated value of middle image was 133 μm and the bottom one was 344 μm. OCT image could guide the position and depth of external electrode to stimulate exact spot of sample.

Figure 1-10 presented a time series of mapping images of neuronal response caused by electrical stimulation. External needle electrode expressed by white triangle on the image and the neuronal activities was displayed continuously in time order. At first image, blue colored map signal was caused by negative stimulation of electrode. After 2 ms, the position near the spot of electrical stimulation was induced. Neuronal signals were evoked in CA1 at 103 ms with +87 μV and then, positive and negative values were evoked alternately in DG. Through this experiment, we found that IGRS is a very useful tool to check the sample defects as well as to confirm the position and depth of external electrode in electrical stimulation.

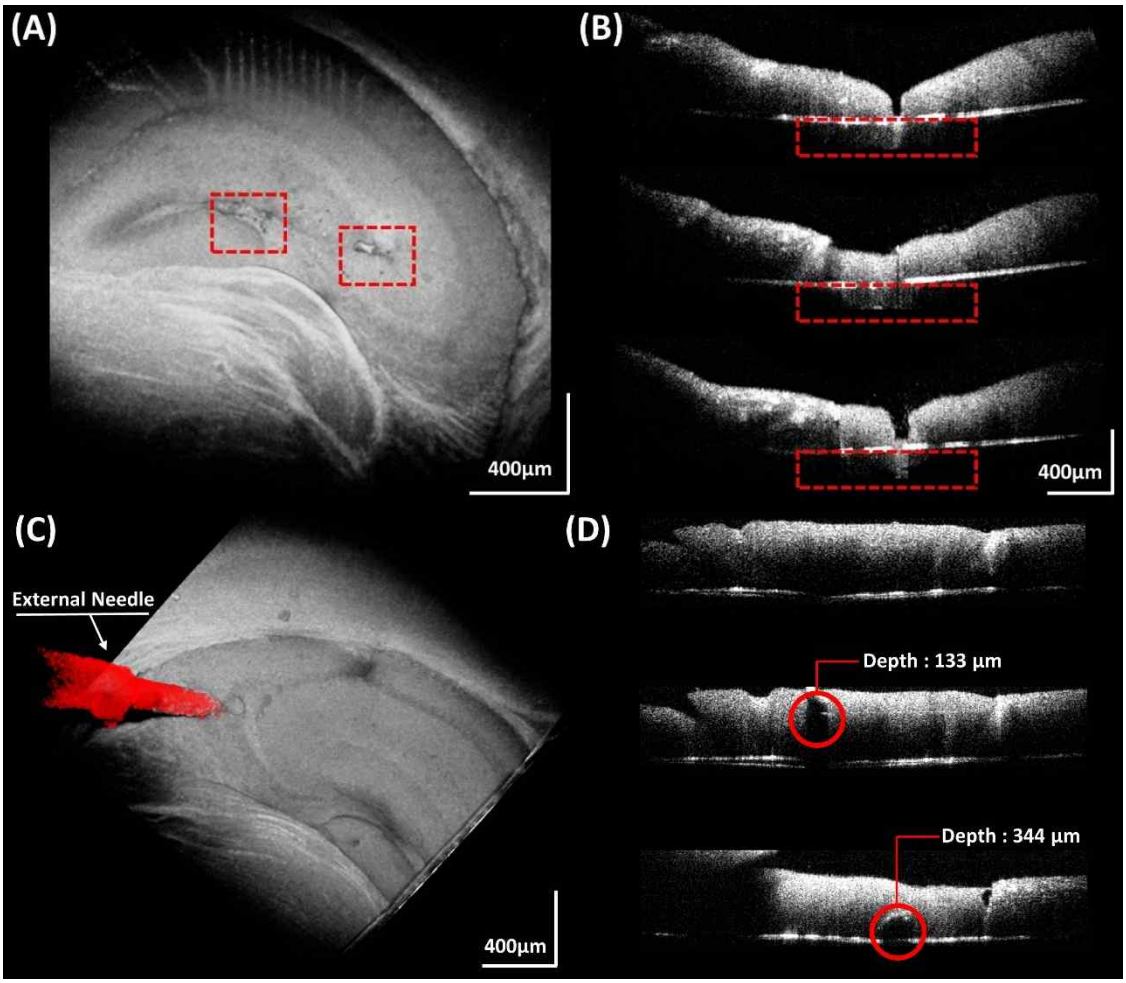

Figure 1-9. Sample defect and calculation for the depth of external needle using IGRS.

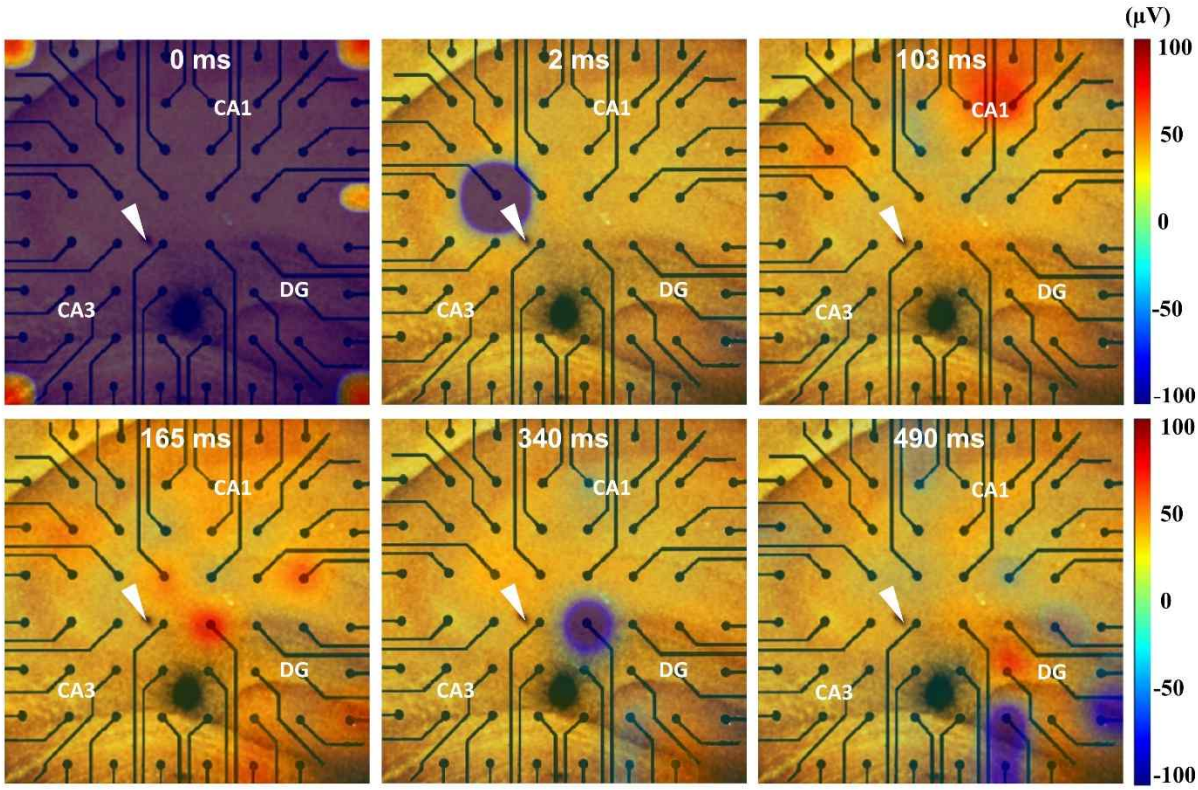

Figure 1-10. Temporal and spatial mapping images caused by electrical stimulation

2.4. Discussion

MEA have been widely used as indispensable tool to acquire neuronal activities and evaluate neuronal connectivity. However, there are limits to the extent to which signals couldn't be accurately matched with the physical location of the sample and they couldn't be analyzed at a glance. These provided a challenge for the widespread use of MEA in neuroscience field and it could affect to the originated position of neuronal activities and the information of signal flow.

Thus, in this study, we obtained accurate 3D structure information of the sample and electrodes using the OCT imaging technology. Based on this, the spatial reliability between the measuring device and the sample was established. Also, received signals were mapped on the actual image in the chronological order.

Although there was a distortion of data in interpolation step, the accuracy will be improved if we change the MEA which have narrow distance between the electrodes. That way, the resolution of signals acquired from MEA will be raised enough to cover the error. And the device which have higher resolution have been developed in various process methods and materials. Furthermore, when materials are changed, there may be problems with imaging. However, IGRS will be not affected to obtaining 3D information of brain tissue because OCT imaging technology is non-invasive imaging modality. Therefore, it can be considered free-material monitoring system.

In conclusion, IGRS will be very useful to find the effect of drug and toxin as well as to apply a various stimulation technique for neurons like electrical and optical stimulation method. Because it can provide the dynamic change of neuronal activities at specific position using visual medium. Also, it is possible to enhance understanding of neuronal circuit because it can be observed with signal flow and the actual sample image of the brain slice. We believe that IGRS is applicable to various neuronal experiments and will be useful in this field.

Ⅲ. Single Photon Stimulation For Neuronal Activities Using a Ball Lensed Probe With Visible Light

3.1. Introduction

In neuroscience, the connection of neuronal network is important for understanding structural and functional distribution of brain **[34-36]**. To date, electrical stimulation and recording methods have been used as indispensable tool to evaluate neuronal connectivity. Recently, various optical methods have been introduced as an alternative technique, due to its spatial resolution, multiple stimulation as well as non-invasive manner for single neuron manipulation **[37-39]**. Among optical stimulation methods, single-photon stimulation based on caged glutamate is one of well-known technique which uses photolysis in order to release neurotransmitter **[40-44]**. Although it offers high yield and simple stimulation procedure compared to existing electrical method, it has restriction to utilize various neuronal research because of complexity to find optimal experiment conditions varying the optical wavelength and type of glutamate. In preliminary study, we propose the photolysis equation to adjust experimental conditions and predict corresponding neuronal activity. Our equation consists of the concentration of glutamate and optical stimulation parameters which include wavelength, intensity, and exposure time. Furthermore, we compare the numerical and experiment results with given stimulation parameters **[8]**.

However, several problems and limitations were remained like high expense and low accessibility to other system. Therefore, we developed probe-based optical stimulator which has various advantages of accessibility, cost efficiency, portability. Before the manufacturing of it, optical path of fiber was simulated by ABCD matrix to design beam diameter and wording distance. In addition, ball lensed probe was controlled by piezo motor to induce photolysis of caged glutamate.

3.2. Methods and Materials

3.2.1 Photolysis of caged glutamate in single-photon stimulation

L-glutamate is the most abundant excitatory neurotransmitter in the nervous system **[45-46]**, as its release at the synapses deliver electrical signals chemically from presynaptic to postsynaptic neurons. Therefore, excitatory chemical synapses evoke an excitatory postsynaptic potential (EPSP) on the postsynaptic neurons. Photolysis of caged glutamate as one of photo-stimulation techniques mimics synaptic activation by photo-release of L-glutamate **[43]**. In order to enhance the comprehension of our experiment, **Figure 2-1** described glutamate receptor and the mechanisms of glutamatergic excitation in the nerve synapses briefly **[47-48]**.

Action potential in the presynaptic neuron induces the release of glutamate from the presynaptic terminals. The released glutamate binds to glutamate receptor located at the postsynaptic membrane. AMPA and kainite receptors permit conduction of sodium ions, which depolarize EPSP of the postsynaptic cell. The depolarization through the above receptors initiate the relief of magnesium ions that block NMDA receptors, and NMDA-receptor mediate a calcium ion in the extracellular environment. Finally, calcium which is a central messenger molecule activates second-messenger signaling pathways in the postsynaptic cell, retaining persistent activation of two protein kinases and taking in glutamate actively on the postsynaptic neuron **[49-50]**. In summary, **Figure 2-1** explains the mechanisms of glutamatergic synapses in the axon terminals.

In this study, principle of single-photon stimulation was released glutamate by applied visible light through ball lensed probe. There are two kinds of caged compounds which are pre-chemicals to be released into glutamate like MNI-glutamate and Rubi-glutamate as shown in **Figure 2-2**. When MNI-glutamate and Rubi-glutamate were exposed by excitation wavelength, glutamate connected amine group with other bulk compounds was divided. Afterward, released glutamate could be a neurotransmitter to stimulate neighbor neurons at excitation point.

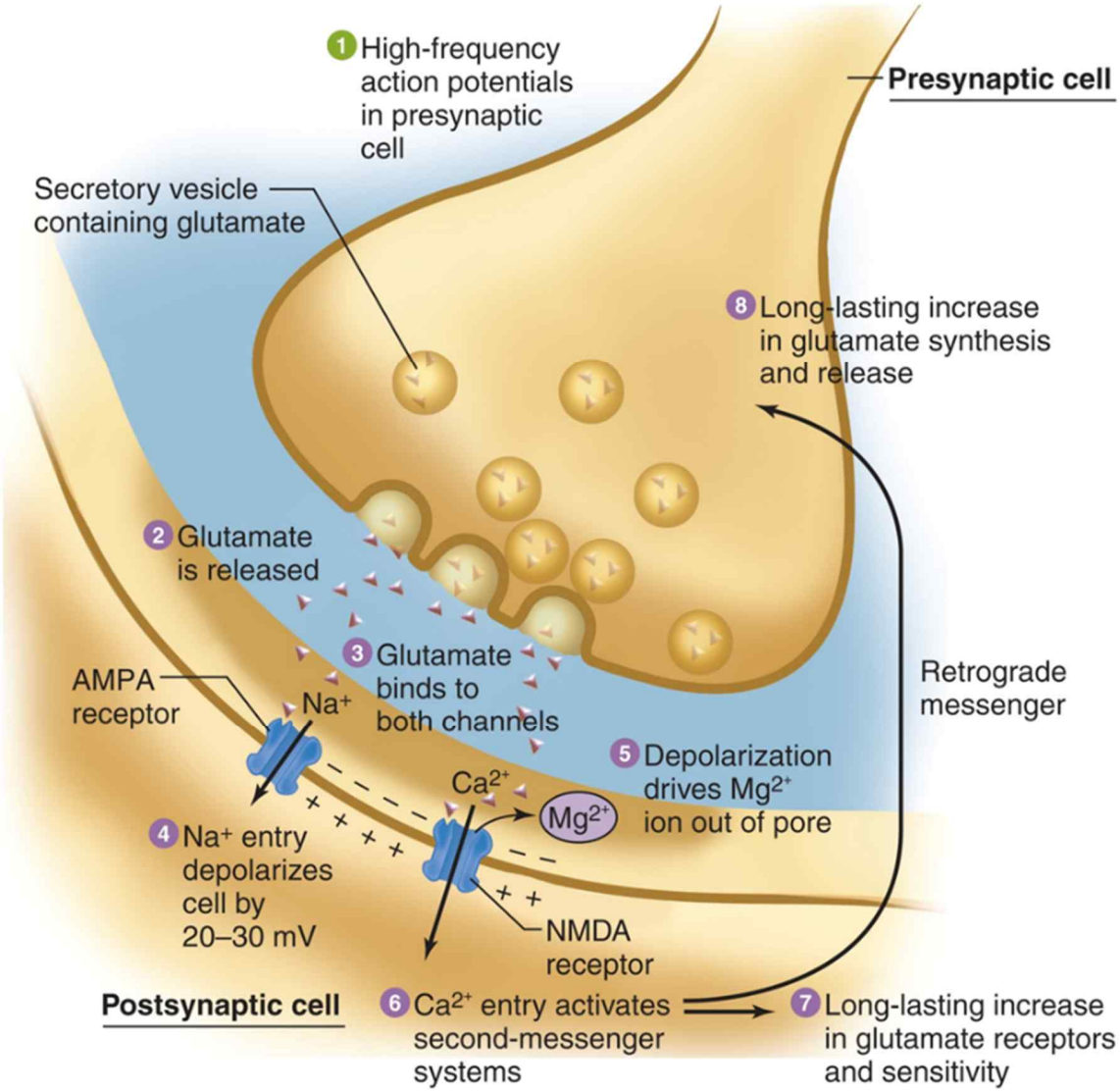

Figure 2-1. The mechanisms of glutamatergic synapses in the axon terminals [47]

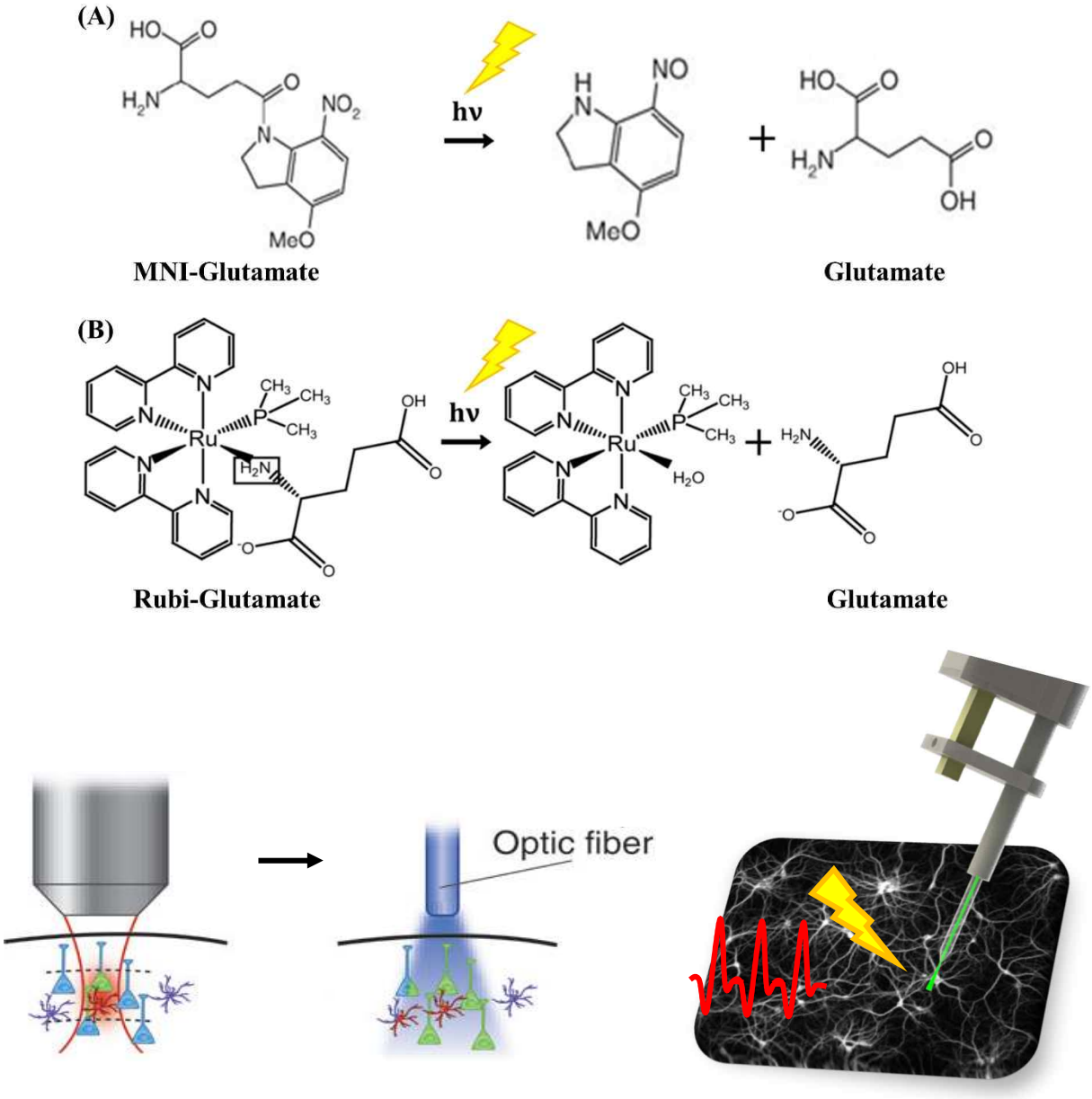

Figure 2-2. MNI-glutamate and Rubi-glutamate used in this research as pre-chemical and schematic of single-photon stimulation in commercial and optic fiber.

3.2.2 Primary Cell Culture

Hank's Balenced Salt Sodium (HBSS) (Gibco, USA)

B27 supplement (Gibco, USA)

Neurobasal Medium (Gibco, USA)

Sprague-Dawley rats (Hyochang Science, Korea)

Trypsin-EDTA (Gibco, USA)

GlutaMAX™ Supplement (Gibco, USA)

Primocin (InvivoGen, USA)

Micro forceps and micro scissor

Entire experiment and animal handling was carried out according to IACUC regulation in UNIST (UNISTIACUC-17-08). After carbon dioxide (CO_2) anesthesia treatment, primary hippocampal neurons were isolated from rats of embryonic day 17 ~ 18. The rat brains were removed from the embryos and their hippocampal neurons were rapidly dissected from cortex at 4 °C in HBSS. After being dissociated in 0.25 % trypsin–EDTA solution for 15 min in a water bath at 37 °C, DMEM containing 10% horse serum was added into solution to stop the effect of trypsin. Then, the cells were transferred into culture media containing neurobasal media supplemented with B27 (20 mL/L), GlutaMax (2.5 mL/L) and Primocin (100 μg/ml). The neurons were incubated at 37 °C in air containing 5 % CO_2 for 7 ~ 14 days before experiment.

3.3. Results

3.3.1 Fiber Optic Simulation & Measured Data

Fiber optic simulation was processed by MATLAB (MathWorks, USA) using ABCD matrix **[51-53]**. In order to obtain for the beam waist and working distance (WD), Gaussian optics can be expressed as below:

$$q = z + iz_0$$

z represents the distance of the given transverse plane from focal point and z_0 means the Rayleigh range. When a Gaussian beam expressed by q_1 passes through optical components represented by an ABCD matrix, output q_2 of the beam is written as

$$q_2 = \frac{Aq_1 + B}{Cq_1 + D}$$

In our experiment, we used a single mode fiber with a Gaussian beam. Beam waist has a minimum value because it is at focal length. Therefore, parameter can be represented by:

$$q_1 = iz_{01} = \frac{\pi n_f w_0^2}{\lambda} = \frac{n_f i}{a_0} = \frac{i}{a}$$

z_{01} is the Rayleigh range of the initial Gaussian beam. n_f, w_0, and λ means the refractive index of the fiber core, the beam radius at the fiber core, and the wavelength of the guided beam. The beam parameters of the propagating light in a probe is written as

$$q_2 = \frac{AC + BDa^2}{C^2 + D^2a^2} + i\frac{(AD - BD)a^2}{C^2 + D^2a^2}$$

From this equation, the WD can be calculated by taking the negative of real part as shown in z_w

$$z_w = -\frac{AC + BDa^2}{C^2 + D^2a^2}$$

The imaginary part of q_2 means the new Rayleigh range z_{02} at the focal point, which represents the beam waist at the focal point.

$$z_{02} = \frac{(AD - BD)a^2}{C^2 + D^2a^2}$$

Finally, the beam waist in terms of the initial waist can be calculated as w_{02}

$$w_{02} = w_{01}\left(\frac{n_f a z_{02}}{n_s}\right)^{1/2}$$

w_{01}, n_s represents the initial beam waist in the input plane and the refractive index of the medium (water or air) at the output plane.

The parameters of simulation:

$n_{sil} = 1.467287$ (Refractive index of the silica)

$n_{air} = 1.0003$ (Refractive index of the air)

$n_{water} = 1.333333$ (Refractive index of the water)

$l_{csf} = 1000$ (Length of the CSF; μm)

$\lambda = 0.43$ (Wavelength of laser module; μm)

$w_0 = 3.3$ (Initial beam waist from the SMF; μm)

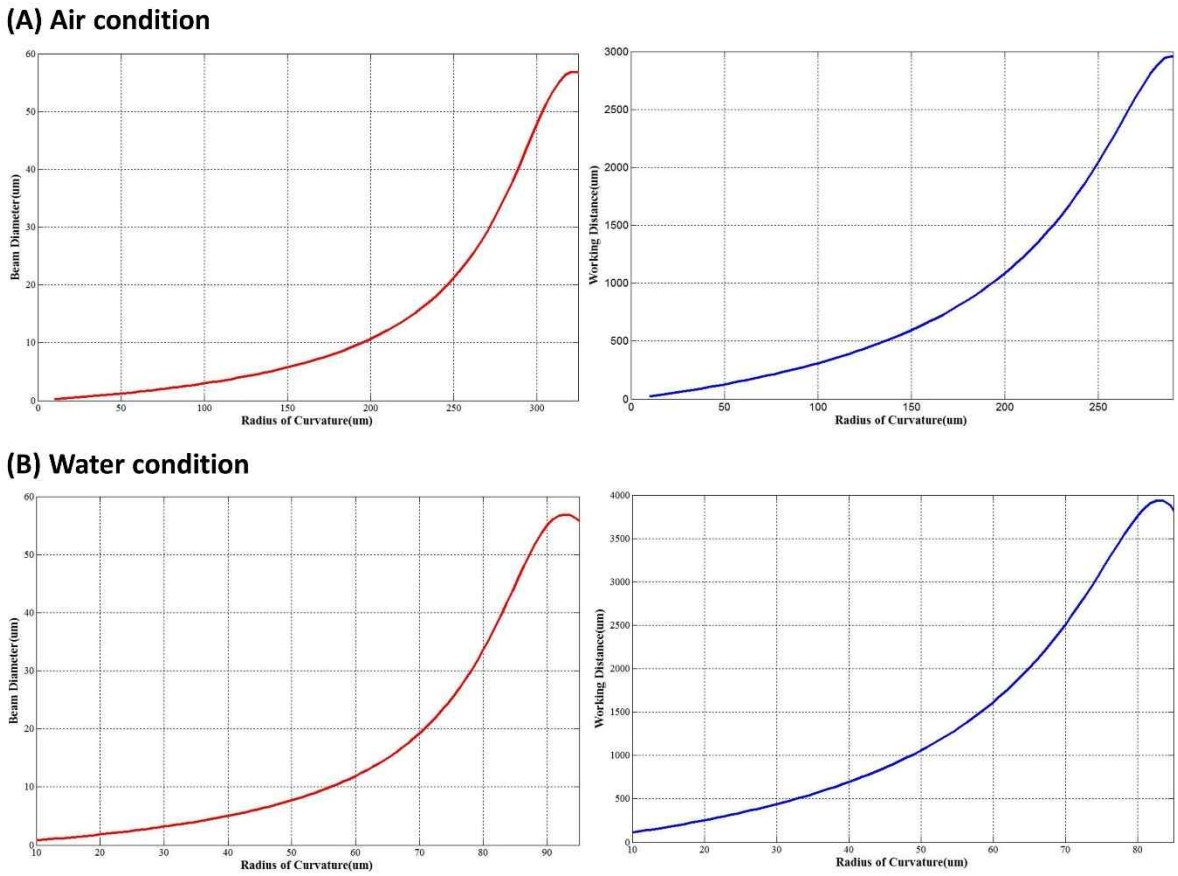

Figure 2-3. The results of fiber optic simulation with air and water medium.

3.3.2 Ball Lensed Stimulator Manufacturing

Schematic diagram of manufacturing step and image of ball lensed fiber was shown in **Figure 2-3**. There are two kinds of materials to build a ball lensed fiber, single mode fiber (SMF) and coreless silica fiber (CSF). SMF (diameter of core/cladding: 3.3 μm / 125 μm) is an optical fiber designed to carry light only directly down the fiber in transverse axis and CSF is used to expand the beam diameter as a spacer. When ball lensed fiber was fabricated, there were Clearing, Fusion, Cleave, Terminal steps.

At first, outer jacket and coating of the SMF must be stripped by wire stripper since SMF consists of fiber core, glass cladding, buffer coating and outer jacket. Then, the end of fiber was cut by fiber cleaver (Fiberoptic, China) to be neatly cut off. And it was put on the stage of fusion splicer (Fitel, Japan) and debris clearing step was processed under 10 mV of arc power and 50 ms duration time.

In second step, CSF which was also neatly cut off by fiber cleaver was loaded on the opposite stage of the SMF. After one more debris clearing step, the end of SMF and CSF was aligned straightly by controlling of x and y axis motor. Then, two kinds of fibers were fused under 110 mV of arc power and 950 ms of duration time.

After that, SMF-CSF fused fiber was cut by fiber cleaver at the point where CSF length could be 1000 μm as we simulated in **Figure 2-3**. After that, debris clearing step must be processed. Finally, remained fiber was aligned between two discharging probes to be fully affected by them. Arc discharge under 90 mV of arc power and 650 ms of duration time was applied to manufacture ball lensed optical fiber.

Figure 2-5 shows that Schematic diagram and the image of ball lensed stimulator with a piezo motor. The hardware of stimulator was designed using SolidWorks (Dassault System, France) and built by 3D printer. Fully developed fiber and piezo motor (Faulhaber, Germany) to control focal point were assembled with hardware of stimulator and the real image of it as shown in **Figure 2-5 (C)**.

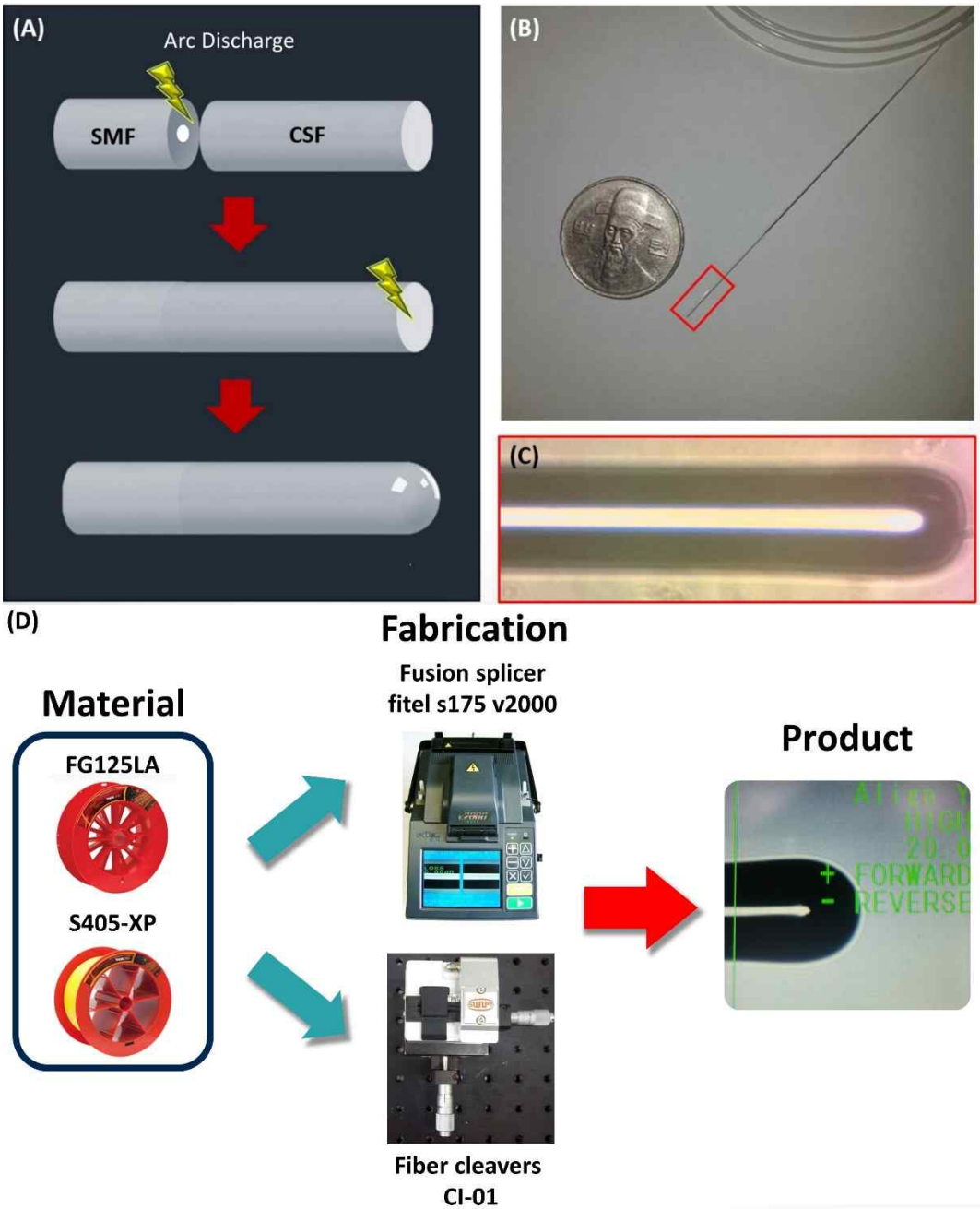

Figure 2-4. Schematic diagram of manufacturing step and image of ball lensed fiber.

(A) Fiber fusion and ball lens were built by arc discharge (SMF; single mode fiber, CSF; coreless silica fiber). (B, C) The end of ball lensed fiber was compared with a coin expanded image. (D) Ball lensed optical fiber was made from SMF (S405-XP, Thorlabs), CSF (FG125LA, Thorlabs) and fabricated by fusion splicer (Fitel, Japan).

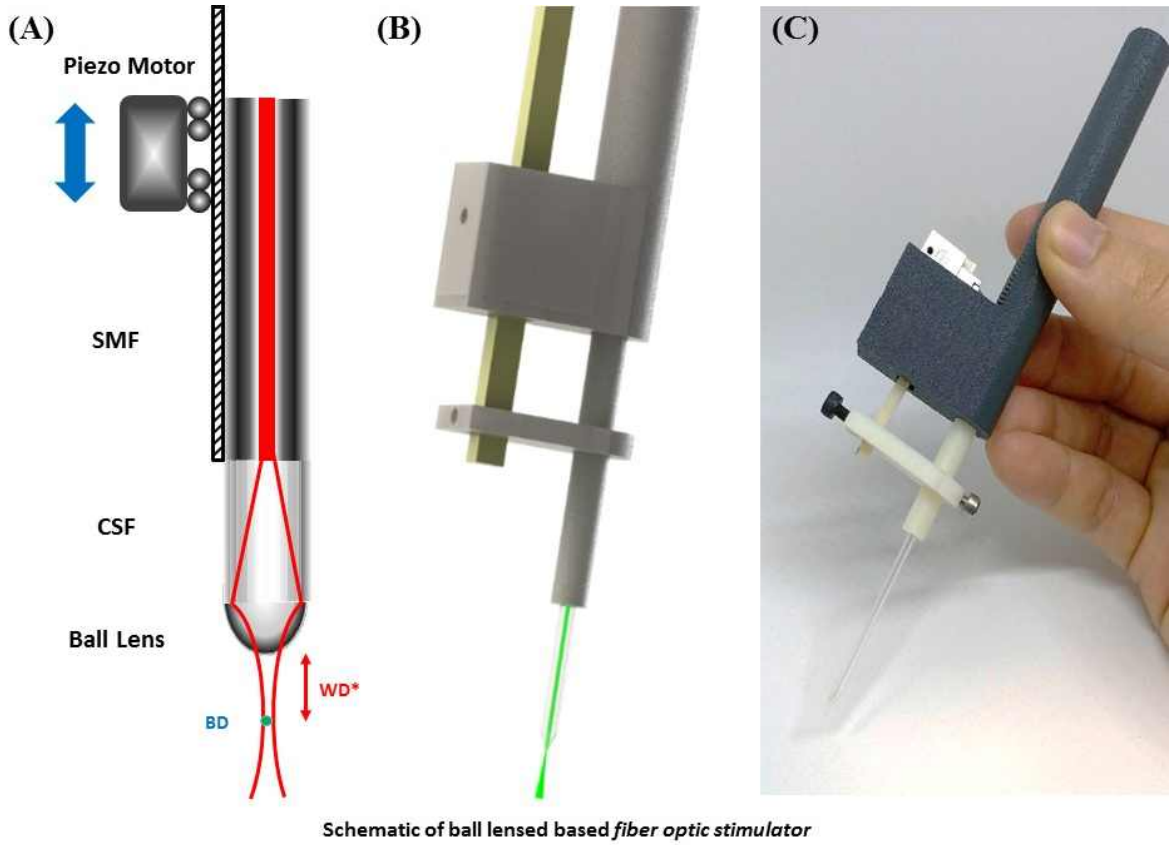

Figure 2-5. Schematic diagram and the image of ball lensed stimulator with a piezo motor.

3.4. Discussion

In neuroscience, there are lots of optical stimulation methods which offers high yield and simple stimulation procedure compared to electrical methods. Among optical stimulation methods, single-photon stimulation based on caged glutamate is well-known technique which uses photolysis to release glutamate as a neurotransmitter. Although its characteristics are spatial resolution, multiple stimulation as well as non-invasive manner, commercial stimulation technique has several weakness points than probe-based optical stimulator.

Firstly, many researchers used UV wavelength as a light source though it caused damage to the neuron cells. In preliminary study, we propose the photolysis equation to adjust experimental conditions and predict corresponding neuronal activities with a visible wavelength. Therefore, we used the visible light of 405 nm, 450 nm, and 520 nm wavelength in instead of UV to prevent cell damage. In order to expect and manufacture ball lensed fiber, we simulate beam diameter and working distance at a focal point.

In addition, we developed probe-based optical stimulator which has various advantages of accessibility, cost efficiency, portability because it consisted of replaceable laser modules and piezo motor. Differently from bulk light source, our device was just composed of fiber type, portable laser module, and piezo motor. Therefore, probe-based optical stimulator is highly accessible, portable, and has low cost to study optical stimulation for primary cultured neurons.

Ⅳ. Conclusion

We introduced IGRS combined MEA and OCT which enable automated and intuitive registration of neuronal activities on brain structure image. The performance of IGRS was evaluated by presenting the efficient spatial and temporal interpretation regarding APs and LFPs of hippocampal region in brain slice. Through our pilot study, we convinced that IGRS and mapping protocol are well adaptable tool to high-throughput MEA system and massive data process.

In addition, we developed ball lensed optical stimulator to apply the focused beam inducing neuronal activities. The parameters of fiber components and manufacturing conditions were simulated, and the hardware of stimulator with piezo motor was developed. Furthermore, the spec of stimulator was evaluated.

In conclusion, we introduced IGRS for monitoring of neuronal activities in brain slice and optical probe for stimulating of primary cultured neuron.

References

[1] Selkoe, D. J., Alzheimer's disease is a synaptic failure. *Science* **2002,** *298* (5594), 789-791.

[2] Mormino, E.; Kluth, J.; Madison, C.; Rabinovici, G.; Baker, S.; Miller, B.; Koeppe, R.; Mathis, C.; Weiner, M.; Jagust, W., Episodic memory loss is related to hippocampal-mediated β-amyloid deposition in elderly subjects. *Brain* **2008,** *132* (5), 1310-1323.

[3] Dauer, W.; Przedborski, S., Parkinson's disease: mechanisms and models. *Neuron* **2003,** *39* (6), 889-909.

[4] Vezzani, A.; Granata, T., Brain inflammation in epilepsy: experimental and clinical evidence. *Epilepsia* **2005,** *46* (11), 1724-1743.

[5] Morris, R.; Garrud, P.; Rawlins, J. a.; O'Keefe, J., Place navigation impaired in rats with hippocampal lesions. *Nature* **1982,** *297* (5868), 681-683.

[6] Burgess, N.; Maguire, E. A.; O'Keefe, J., The human hippocampus and spatial and episodic memory. *Neuron* **2002,** *35* (4), 625-641.

[7] Frankland, P. W.; Bontempi, B., The organization of recent and remote memories. *Nature Reviews Neuroscience* **2005,** *6* (2), 119-130.

[8] Lee, J., Numerical analysis of neuronal responses for photolysis of MNI and Rubi caged glutamate. **2017**.

[9] Buzsáki, G.; Anastassiou, C. A.; Koch, C., The origin of extracellular fields and currents—EEG, ECoG, LFP and spikes. *Nature reviews neuroscience* **2012,** *13* (6), 407-420.

[10] Buzsáki, G.; Draguhn, A., Neuronal oscillations in cortical networks. *science* **2004,** *304* (5679), 1926-1929.

[11] Vandermaelen, C.; Aghajanian, G., Electrophysiological and pharmacological characterization of serotonergic dorsal raphe neurons recorded extracellularly and intracellularly in rat brain slices. *Brain research* **1983,** *289* (1), 109-119.

[12] Morin, F. O.; Takamura, Y.; Tamiya, E., Investigating neuronal activity with planar microelectrode arrays: achievements and new perspectives. *Journal of bioscience and bioengineering* **2005,** *100* (2), 131-143.

[13] Obien, M. E. J.; Deligkaris, K.; Bullmann, T.; Bakkum, D. J.; Frey, U., Revealing neuronal function through microelectrode array recordings. *Frontiers in neuroscience* **2015,** *8*, 423.

[14] Stett, A.; Egert, U.; Guenther, E.; Hofmann, F.; Meyer, T.; Nisch, W.; Haemmerle, H., Biological application of microelectrode arrays in drug discovery and basic research. *Analytical and bioanalytical chemistry* **2003,** *377* (3), 486-495.

[15] Frey, U.; Egert, U.; Heer, F.; Hafizovic, S.; Hierlemann, A., Microelectronic system for high-resolution mapping of extracellular electric fields applied to brain slices. *Biosensors and Bioelectronics* **2009,** *24* (7), 2191-2198.

[16] Müller, J.; Ballini, M.; Livi, P.; Chen, Y.; Radivojevic, M.; Shadmani, A.; Viswam, V.; Jones, I. L.; Fiscella, M.; Diggelmann, R., High-resolution CMOS MEA platform to study neurons at subcellular, cellular, and network levels. *Lab on a Chip* **2015,** *15* (13), 2767-2780.

[17] Bikson, M.; Inoue, M.; Akiyama, H.; Deans, J. K.; Fox, J. E.; Miyakawa, H.; Jefferys, J. G., Effects of uniform extracellular DC electric fields on excitability in rat hippocampal slices in vitro. *The Journal of physiology* **2004,** *557* (1), 175-190.

[18] Hutzler, M.; Lambacher, A.; Eversmann, B.; Jenkner, M.; Thewes, R.; Fromherz, P., High-resolution multitransistor array recording of electrical field potentials in cultured brain slices. *Journal of neurophysiology* **2006,** *96* (3), 1638-1645.

[19] Ferrea, E.; Maccione, A.; Medrihan, L.; Nieus, T.; Ghezzi, D.; Baldelli, P.; Benfenati, F.; Berdondini, L., Large-scale, high-resolution electrophysiological imaging of field potentials in brain slices with microelectronic multielectrode arrays. *Frontiers in neural circuits* **2012,** *6*.

[20] Huang, D.; Swanson, E. A.; Lin, C. P.; Schuman, J. S.; Stinson, W. G.; Chang, W.; Hee, M. R.; Flotte, T.; Gregory, K.; Puliafito, C. A., Optical coherence tomography. *Science (New York, NY)* **1991,** *254* (5035), 1178.

[21] Fujimoto, J. G., Optical coherence tomography for ultrahigh resolution in vivo imaging. *Nature biotechnology* **2003,** *21* (11), 1361-1367.

[22] Min, E.; Lee, J.; Vavilin, A.; Jung, S.; Shin, S.; Kim, J.; Jung, W., Wide-field optical coherence microscopy of the mouse brain slice. *Optics letters* **2015,** *40* (19), 4420-4423.

[23] Men, J.; Huang, Y.; Solanki, J.; Zeng, X.; Alex, A.; Jerwick, J.; Zhang, Z.; Tanzi, R. E.; Li, A.; Zhou, C., Optical coherence tomography for brain imaging and developmental biology. *IEEE Journal of Selected Topics in Quantum Electronics* **2016,** *22* (4), 120-132.

[24] Chong, S. P.; Merkle, C. W.; Cooke, D. F.; Zhang, T.; Radhakrishnan, H.; Krubitzer, L.; Srinivasan, V. J., Noninvasive, in vivo imaging of subcortical mouse brain regions with 1.7 μm optical coherence tomography. *Optics letters* **2015,** *40* (21), 4911-4914.

[25] Xie, Y.; Harsan, L.-A.; Bienert, T.; Kirch, R. D.; Von Elverfeldt, D.; Hofmann, U. G., Qualitative and quantitative evaluation of in vivo SD-OCT measurement of rat brain. *Biomedical optics express* **2017,** *8* (2), 593-607.

[26] Fejtl, M.; Stett, A.; Nisch, W.; Boven, K.-H.; Möller, A., On micro-electrode array revival: its development, sophistication of recording, and stimulation. *Advances in network electrophysiology* **2006**, 24-37.

[27] Tian, G.-F.; Azmi, H.; Takano, T.; Xu, Q.; Peng, W.; Lin, J.; Oberheim, N.; Lou, N.; Wang, X.; Zielke, H. R., An astrocytic basis of epilepsy. *Nature medicine* **2005,** *11* (9), 973-981.

[28] Doležal, V.; Tuček, S., The effects of 4-aminopyridine and tetrodotoxin on the release of acetylcholine from rat striatal slices. *Naunyn-Schmiedeberg's archives of pharmacology* **1983,** *323* (2), 90-95.

[29] Tibbs, G.; Barrie, A.; Mieghem, F.; McMahon, H. a.; Nicholls, D., Repetitive action potentials in isolated nerve terminals in the presence of 4-aminopyridine: Effects on cytosolic free Ca2+ and glutamate release. *Journal of neurochemistry* **1989,** *53* (6), 1693-1699.

[30] Dingledine, R.; Dodd, J.; Kelly, J., The in vitro brain slice as a useful neurophysiological preparation for intracellular recording. *Journal of neuroscience methods* **1980,** *2* (4), 323-362.

[31] Yeckel, M. F.; Berger, T. W., Feedforward excitation of the hippocampus by afferents from the entorhinal cortex: redefinition of the role of the trisynaptic pathway. *Proceedings of the National Academy of Sciences* **1990,** *87* (15), 5832-5836.

[32] Benes, F. M., Evidence for altered trisynaptic circuitry in schizophrenic hippocampus. *Biological psychiatry* **1999,** *46* (5), 589-599.

[33] Jones, M. W.; McHugh, T. J., Updating hippocampal representations: CA2 joins the circuit. *Trends in neurosciences* **2011,** *34* (10), 526-535.

[34] Bassett, D. S.; Bullmore, E., Small-world brain networks. *The neuroscientist* **2006,** *12* (6), 512-523.

[35] Park, H.-J.; Friston, K., Structural and functional brain networks: from connections to cognition. *Science* **2013,** *342* (6158), 1238411.

[36] Bressler, S. L.; Menon, V., Large-scale brain networks in cognition: emerging methods and principles. *Trends in cognitive sciences* **2010,** *14* (6), 277-290.

[37] Callaway, E. M.; Yuste, R., Stimulating neurons with light. *Current opinion in neurobiology* **2002,** *12* (5), 587-592.

[38] Zhang, F.; Wang, L.-P.; Boyden, E. S.; Deisseroth, K., Channelrhodopsin-2 and optical control of excitable cells. *Nature methods* **2006,** *3* (10), 785-792.

[39] Zhang, F.; Gradinaru, V.; Adamantidis, A. R.; Durand, R.; Airan, R. D.; De Lecea, L.; Deisseroth, K., Optogenetic interrogation of neural circuits: technology for probing mammalian brain structures. *Nature protocols* **2010,** *5* (3), 439-456.

[40] Ellis-Davies, G. C.; Matsuzaki, M.; Paukert, M.; Kasai, H.; Bergles, D. E., 4-Carboxymethoxy-5, 7-dinitroindolinyl-Glu: an improved caged glutamate for expeditious ultraviolet and two-photon photolysis in brain slices. *Journal of Neuroscience* **2007,** *27* (25), 6601-6604.

[41] Banerjee, A.; Grewer, C.; Ramakrishnan, L.; Jäger, J.; Gameiro, A.; Breitinger, H.-G. A.; Gee, K. R.; Carpenter, B. K.; Hess, G. P., Toward the development of new photolabile protecting groups that can rapidly release bioactive compounds upon photolysis with visible light. *The Journal of organic chemistry* **2003,** *68* (22), 8361-8367.

[42] Shembekar, V. R.; Chen, Y.; Carpenter, B. K.; Hess, G. P., A protecting group for carboxylic acids that can be photolyzed by visible light. *Biochemistry* **2005,** *44* (19), 7107-7114.

[43] Ellis-Davies, G. C., A chemist and biologist talk to each other about caged neurotransmitters. *Beilstein journal of organic chemistry* **2013,** *9*, 64.

[44] Callaway, E. M.; Katz, L. C., Photostimulation using caged glutamate reveals functional circuitry in living brain slices. *Proceedings of the National Academy of Sciences* **1993,** *90* (16), 7661-7665.

[45] Danbolt, N. C., Glutamate uptake. *Progress in neurobiology* **2001,** *65* (1), 1-105.

[46] Trigo, F. F.; Corrie, J. E.; Ogden, D., Laser photolysis of caged compounds at 405nm: Photochemical advantages, localisation, phototoxicity and methods for calibration. *Journal of neuroscience methods* **2009,** *180* (1), 9-21.

[47] Specht, A.; Bolze, F.; Nicoud, J. F.; Goeldner, M., Characterization of one-and two-photon photochemical uncaging efficiency. *Chemical Neurobiology: Methods and Protocols* **2013**, 79-87.

[48] Meldrum, B. S., Glutamate as a neurotransmitter in the brain: review of physiology and pathology. *The Journal of nutrition* **2000,** *130* (4), 1007S-1015S.

[49] Vignes, M.; Collingridge, G. L., The synaptic activation of kainate receptors. *Nature* **1997,** *388* (6638), 179-182.

[50] Dingledine, R.; Borges, K.; Bowie, D.; Traynelis, S. F., The glutamate receptor ion channels. *Pharmacological reviews* **1999,** *51* (1), 7-62.

[51] Jung, W.; Benalcazar, W.; Ahmad, A.; Sharma, U.; Tu, H.; Boppart, S. A., Numerical analysis of gradient index lens–based optical coherence tomography imaging probes. *Journal of biomedical optics* **2010,** *15* (6), 066027-066027-10.

[52] Silfvast, W. T., *Laser fundamentals*. Cambridge university press: 2004.

[53] Gomez-Reino, C.; Perez, M. V.; Bao, C., *Gradient-index optics: fundamentals and applications*. Springer Science & Business Media: 2012.